Tribology Letters (2022) 70:63
https://doi.org/10.1007/s11249-022-01605-3

ORIGINAL PAPER

Synthesis of MXene-Based Self-dispersing Additives for Enhanced Tribological Properties

Changzhi Zhou[2] · Zhangpeng Li[1,3,4] · Shuwen Liu[1,4] · Limin Ma[1] · Tianrong Zhan[2] · Jinqing Wang[1]

Received: 2 February 2022 / Accepted: 22 April 2022 / Published online: 13 May 2022

Abstract

As an emerging class of the two-dimensional (2D) materials, MXenes exhibit excellent antifriction and wear resistance potential in lubrication systems. However, as a lubricant additive, their stable dispersion in base oils remains a great challenge. Optimizing the microstructure has previously been demonstrated to be an effective strategy to improve the dispersibility of inorganic materials in oil-based lubricants. In this work, the structural modulation of MXene through in-situ growth of hydroxysalts (HS) to form a heterostructure was achieved. Compared with pristine MXene and HS, the dispersion stability of MXene/HS composite in poly-α-olefin-10 (PAO-10) base oil was significantly improved due to the self-dispersion and restacking-resistant properties of the heterostructure. Additionally, the lubrication performance of the obtained composite as an additive in PAO-10 was investigated. The results showed that the coefficient of friction of the oil sample containing the MXene/HS composite was steadily maintained at approximately 0.12 under four different loads of 200, 250, 300, and 350 N (corresponding to maximum Hertz contact pressures of 2.72, 2.9, 3.12, and 3.28 GPa, respectively). Moreover, the wear track width, wear scar diameter, and wear volume were reduced by 49.1%, 49.4%, and 82.0%, respectively. This study introduces a viable pathway to transform non-lipophilic $Ti_3C_2T_x$ MXene into an attractive lubricant additive with excellent self-dispersing ability through structural regulation.

Graphical Abstract

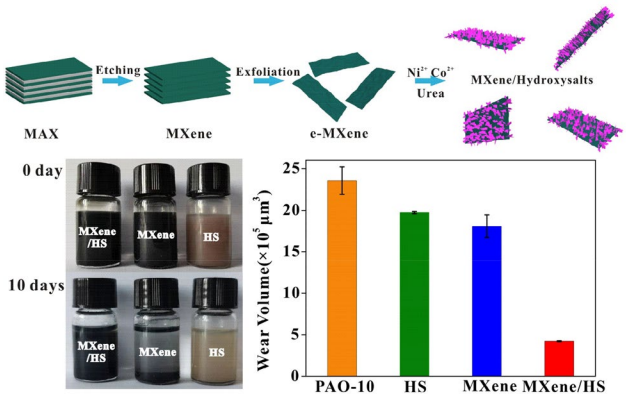

Keywords MXene · Hydroxysalt · Self-dispersing ability · Nanocomposite additive · Lubrication

1 Introduction

The ubiquity of friction and wear phenomena presents an adverse impact on normal mechanical operation, causing inevitable challenges including energy crises and environmental emission issues [1, 2]. In this dilemma, exploring

✉ Zhangpeng Li
zhangpengli@licp.cas.cn

✉ Tianrong Zhan
trzhan@qust.edu.cn

Extended author information available on the last page of the article

novel lubrication materials has become a top priority. Current oil-based lubrication is far from perfect as the working conditions become more complicated. For achieving ideal lubricating performance, introducing appropriate additives is an effective measure. A certain amount of additives not only improves the anti-wear and extreme pressure properties of base oils, but also plays a vital role in the corrosion and oxidation resistance of the base oil [3]. Currently, two-dimensional (2D) materials as lubricant additives have been extensively explored in tribology [4–7]. The layered structure and high specific surface area [8] enable them to exert an interlayer shear mechanism and easy adsorption on the friction pair surface. Compared to traditional organic lubricant additives such as zinc dialkyldithophosphate (ZDDP) and molybdenum dithiocarbamate (MoDTC), 2D materials with good chemical stability ensure low toxicity and minimal harmful emissions, in line with the requirement of sustainable development. Typically, graphene, h-BN, layered double hydroxide (LDH), MXene, and other 2D nanomaterials exhibit excellent lubrication properties in terms of friction reduction and wear resistance [9–14].

MXene is an emerging class of layered 2D nanomaterial and has attracted tremendous attention since its discovery in 2011. Owing to superior thermal stability, electromagnetic properties, and mechanical performance [15], it has been commonly employed in the field of biomedicine [16], energy storage [17, 18], catalysis [19], and lubrication [20, 21]. Compared to most of other 2D materials, MXene is easy to meet the required performance through modification due to abundant functional groups (–OH, =O, –F) exist on the surface. Moreover, merits of chemical and structural diversity, easy-to-shear ability, and enhanced bonding characteristics make MXene as a promising candidate for tribological applications. For instance, Grützmacher et al. [22] fabricated a 100 nm-thick homogeneous multilayer $Ti_3C_2T_x$ MXene coating as a solid lubricant and emphasized that the wear life of $Ti_3C_2T_x$ MXene outperforms other 2D nanomaterials. In addition, Marian et al. [23] deposited MXene coating on the bearing washer raceways by drop-casting method and confirmed that the general performance of MXene is superior to state-of-the-art solid lubricants (diamond-like carbon and MoS_2). Overall, MXene holds great potential in lubrication and shows unique tribological advantages over other 2D materials [24, 25]. Similarly, reports of MXene as additives have been gradually excavated in recent years. Nevertheless, the poor dispersion stability of MXene in oil-based lubricants has often been emphasized in previous works. Thus, numerous efforts are required to optimize the dispersibility for achieving desired tribological purposes. For example, some chemical reagents containing polar groups and long alkyl chains, such as dialkyl dithiophosphate (DDP) [26] and tetradecylphosphonic acid (TDPA) [27], were usually used to chemically modify MXene surfaces to make them be uniformly dispersed in the base oils. These organic modifiers can act as a bridge for the affiliation of additives and lubricants, but the introduced chemical modifiers may destroy the initial structure of additives and deteriorate their natural characteristics, thereby affecting the tribological properties [28]. In addition to chemical modification, physical means such as ultrasound [29, 30] can also achieve homogeneous dispersion of additives in oil. Although physical means are convenient to operate under laboratory conditions, secondary agglomeration is still an unsolvable problem for large-scale applications. In contrast, self-dispersed methods [28] not only eliminate the disadvantages of physical and chemical methods, but also can form a homogeneous and stable suspension. Therefore, converting non-lipophilic MXenes into self-dispersed additives is highly desirable.

Structural regulation is an effective method for preparing self-dispersing materials. For example, inspired by the crumpled paper, Dou et al. [31] prepared crumpled graphene ball as high-performance oil-based additive. In contrast to graphite nanosheets, reduced graphene oxide (rGO) sheets, and carbon black, the crumpled graphene balls present unrivaled aggregation-resistant property in PAO-4 oil after structural regulation. Wang et al. [32] fabricated silver/rGO composites via one-step laser irradiation. They found that the removal of oxygen and the decoration of nanoparticles can improve the dispersion stability significantly. Inspired by above achievements, it is logical to develop nanostructured MXene-based lubricant additives for potential tribological applications by regulating their structures. Owing to the rich negative charge on the surface, MXene nanosheets are prone to absorb the positive group to fabricate the corresponding composite material. Hydroxysalts (HS) are inorganic compounds, composing of metal ions, -OH, and other anions (Cl^-, NO_3^-, SO_4^{2-}, and CO_3^{2-}) [33]. Because of the easy control of structure and composition, it has a wide range of applications, including adsorption [34], catalysis [35], and electrochemistry [36]. However, to the best of our knowledge, there have been no reports of HS in tribological applications.

In this work, we designed and prepared MXene/HS nanocomposites as self-dispersed lubricant additives through structural regulation with HS. The formation of HS on MXene not only enlarges the interlayer spacing of MXene but also creates a barrier between the MXene layers to avoid their restacking. Meanwhile, the strong active sites on the surface of MXene prevent aggregation of HS nanosheets. As a result, agglomeration of MXene and HS in the dispersion system is significantly avoided by forming structurally regulated composites. Furthermore, the tribological performance of the mixed oil sample was investigated in detail. The results showed that the MXene/HS composite has efficient friction reduction and anti-wear properties in PAO-10 base oil. This work provides a reference for the design and

synthesis MXene-based composites with self-dispersing properties and enriches the research of MXene as additives for liquid lubricants.

2 Experimental

2.1 Materials

Ti_3AlC_2 powder (MAX, 200 mesh, 98%) was purchased from Beijing Forsman Technology Co., Ltd. Cobalt nitrate hexahydrate ($Co(NO_3)_2{\cdot}6H_2O$) was acquired from Rhawn Reagent. Nickel nitrate hexahydrate ($Ni(NO_3)_2{\cdot}6H_2O$), hydrochloric acid, and citric acid were provided by Sinopharm Reagent Co., Ltd. Lithium fluoride (LiF) was supplied from Macklin. Urea (CH_4N_2O) was obtained from Tianjin Damao Chemical Reagent. PAO-10 oil was supplied from Beijing Sunright Trade Co., Ltd. All chemical reagents were used without further purification.

2.2 Fabrication of $Ti_3C_2T_x$ MXene Aqueous Dispersion

To avoid the hazardous and toxic impact of HF, MILD method was used to prepare MXene [37, 38]. LiF (2 g) was dissolved in a polytetrafluoroethylene (PTFE) liner containing 40 mL HCl (9 M) aqueous solution, followed by the slow addition of 2 g Ti_3AlC_2. The mixture solution was transferred into a water bath and maintained at 35 °C for 24 h with magnetic stirring. After the reaction was completed, the black muddy precipitate was washed with ultrapure water for several times until the pH was close to neutral. Subsequently, the collected paste was dried in a vacuum freeze dryer for at least 48 h to obtain MXene powder. Then, 1 g MXene was dispersed in 250 mL ultrapure water and sonicated for 1 h. The final supernatant (2.8 mg/mL) was obtained by centrifugation at 3500 rpm and stored at 4 °C for the following experiments.

2.3 Fabrication of MXene/HS Composite

$Ni(NO_3)_2{\cdot}6H_2O$ (0.29 g), $Co(NO_3)_2{\cdot}6H_2O$ (0.582 g) and urea (0.8 g) were completely dissolved in a beaker containing 16 mL ultrapure water. 44 mL of the synthesized MXene aqueous solution was poured into it. Thereafter, 0.05 g of citric acid was added to facilitate the anchoring of metal ions on the MXene surface [39], and the whole mixture was magnetically stirred at room temperature for 1 h. Subsequently, the above mixture was transferred into a 100 mL autoclave and heated to 120 °C for 10 h. After centrifugation and washing, the final product was obtained by freeze-drying. For preparing pure HS, the synthesis procedure was the same as MXene/HS composite except for the absence of MXene.

2.4 Characterizations

The crystal structures of the as-synthesized samples were characterized by X-ray diffraction (XRD, Bruker D8 Advance diffractometer, Cu-Kα radiation, $\lambda = 1.5406$ Å) at a scanning rate of 5° min^{-1} and 5–80° angular range. The uneven XRD background of HS was subtracted using Jade 6.0 software. The morphological structures were observed by scanning electron microscopy (SEM, JEOL JSM-7610F, Japan) and transmission electron microscopy (TEM, JEOL JEM-2100, Japan) connected to energy dispersive spectroscopy (EDS). Size distributions of the prepared MXene nanosheets were determined by dynamic light scattering using a potential analyzer (Malvern Zetasizer Nano ZS90, UK). Fourier-transform infrared (FT-IR, Bruker Tensor 27, Germany) spectra were utilized to confirm the surface groups of the materials over a wavenumber range from 4000 to 400 cm^{-1}. X-ray photoelectron spectroscopy (XPS, Thermo ESCALab 250Xi, USA) was carried out using a monochromatic Al-Kα source (10 mA, 14.6 kV). The chamber pressure was about 3×10^{-8} Torr under testing condition. For peak fitting of the high-resolution spectra, Shirley background was chosen over a linear background. The spectra were fitted with a Gaussian–Lorentzian peak model.

2.5 Tribological Tests

Tribological experiments of PAO-10 containing different samples were conducted on an SRV-V tribometer (Optimol) in reciprocating mode. The applied loads were 200, 250, 300, and 350 N (which correspond to maximum Hertz contact pressures of 2.72, 2.93, 3.12, and 3.28 GPa, respectively), and the other test conditions were set to 25 Hz, 1 mm, and 30 min. The extreme pressure property of the PAO-10 oil was evaluated from 50 to 800 N along with the increase of 50 N every 2 min. The steel ball (AISI 52,100 steel, HRC = 60 ± 2, $D = 10$ mm) and the steel disk (AISI 52,100 steel, HRC = 60 ± 2, 24 mm × 7.9 mm) were selected as friction pairs. Both of them were ultrasonically cleaned with petroleum ether and water before the experiment. The wear track width on the steel disk and wear scar diameter on the steel ball were photographed and measured using an optical microscope (Axiocam 208 color). Noncontact 3D optical surface profiler (KLA-Tencor, USA) was used to measure the wear volume, depth of the wear track, and the roughness of wear tracks on the steel disk. The tribological tests were performed at least three times under each condition. According to the Hamrock-Dowson theory, the calculated minimum film thickness under load of 300 N is ~ 32 nm. The test condition was in the boundary lubrication regime

(see in *Supplementary Materials*). The chemical composition of the worn surface was analyzed by XPS (ULVAC-PHI PHI5000 Versaprobe III), which performed at a monochromated Al-Kα 1486.6 eV, voltage of 15 kV, beam of 4.5 mA, and CAE analyzer scan mode. Survey spectra were taken at a 224 eV pass energy with energy step of 1.0 eV, and high-resolution spectra were studied at 69 eV pass energy with energy step of 0.1 eV. The background subtraction method and fitting technique are the same as described in Sect. 2.4.

3 Results and Discussion

Figure 1 illustrates the process for the preparation of the MXene/HS composites, including the formation of MXene, delamination, and *in-situ* growth of hydroxysalts. Typically, the multilayer MXene was synthesized by a top-down method by etching the Al layers with LiF-HCl etchant. And then, multilayered MXene was exfoliated in water by ultrasonication treatment. After centrifugation, exfoliated MXene (e-MXene) suspension containing few-layer MXenes was obtained. As a negatively charged material, MXene nanosheets can firmly absorb Ni^{2+} and Co^{2+}. Later, the decomposition of urea provided an alkaline environment for the formation of HS nanosheets (Supplementary Materials), resulting in MXene/HS nanocomposite.

As presented in Fig. 2 and Fig. S1, the morphology and structural features of the MXene, HS, and MXene/HS composites were identified. It is evident that the obtained multilayered MXene possesses a typical accordion-like structure, indicating that the Al atomic layers have been etched away [40] (Fig. 2a). After ultrasonication in water, thin-delaminated MXene nanosheet was obtained (Fig. 2b). The average size characterized by dynamic light scattering was 344.6 nm (Fig. S2). Remarkably, due to the abundant negatively charged group of MXene, HS nanosheets can be formed on both sides of the sheets. As shown in Fig. 2c, d, HS nanosheets were uniformly anchored on the surface of MXene resulting in rougher surfaces, as well as good separation of MXene nanosheets. Notably, the original sheet-like structure was transformed into a MXene/HS heterostructure by this *in-situ* crystallization process. In contrast, as shown in Fig. S1, serious agglomeration of HS nanoparticles was observed. In the absence of MXene, numerous nanoparticles stacked disorderly to form a sphere with a diameter of approximately 8–10 μm.

TEM images intuitively reflect the successful preparation of HS nanosheets on MXene. As shown in Fig. 3a, b, ultrathin MXene nanosheets were almost transparent and displayed typical smooth structure. Moreover, many nanostructures crawled on the surface of MXenes after growth of HS as shown in Fig. 3c, d. Undoubtedly, negatively charged MXene can provide abundant sites for anchoring Co^{2+} and Ni^{2+} to facilitate the nucleation and growth of HS nanosheets. The EDS mapping results (Fig. S3) proved this inference and illustrated the uniform distribution of C, O, F, Ti, Co, and Ni elements in MXene/HS composite.

To confirm the crystal structure of HS, MXene, and MXene/HS composites, XRD measurements were carried out and the results are presented in Fig. 4. For the HS, diffraction peaks at 10.0°, 17.5°, 26.7°, 33.8°, 39.5°, and 47.3° are assigned to the (100), (020), (220), (221), (231), and (340) planes, which are consistent well with those of its analog ($Co(CO_3)_{0.5}(OH)_{1.0}{\cdot}0.11H_2O$, JCPDS No. 48-0083). This indicates the successfully preparation of HS. Moreover, the typical sharp (002) peak located at 6.5° of MXene indicates that the Al atomic layers were etched away by LiF-HCl etchant, consistent with the SEM observation (Fig. 2a). The

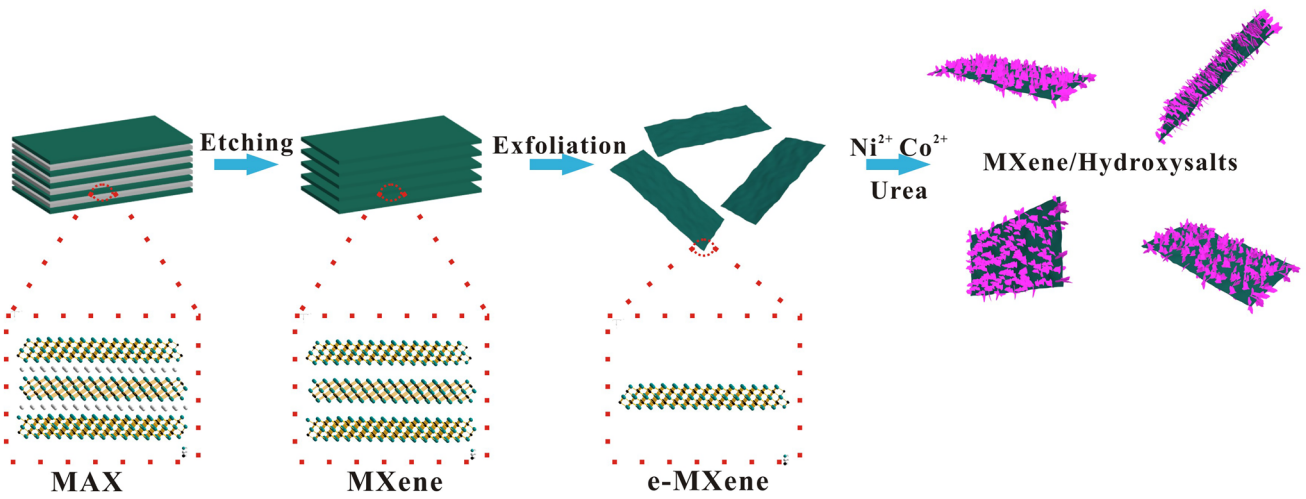

Fig. 1 Schematic diagram of preparation process of MXene/HS composites

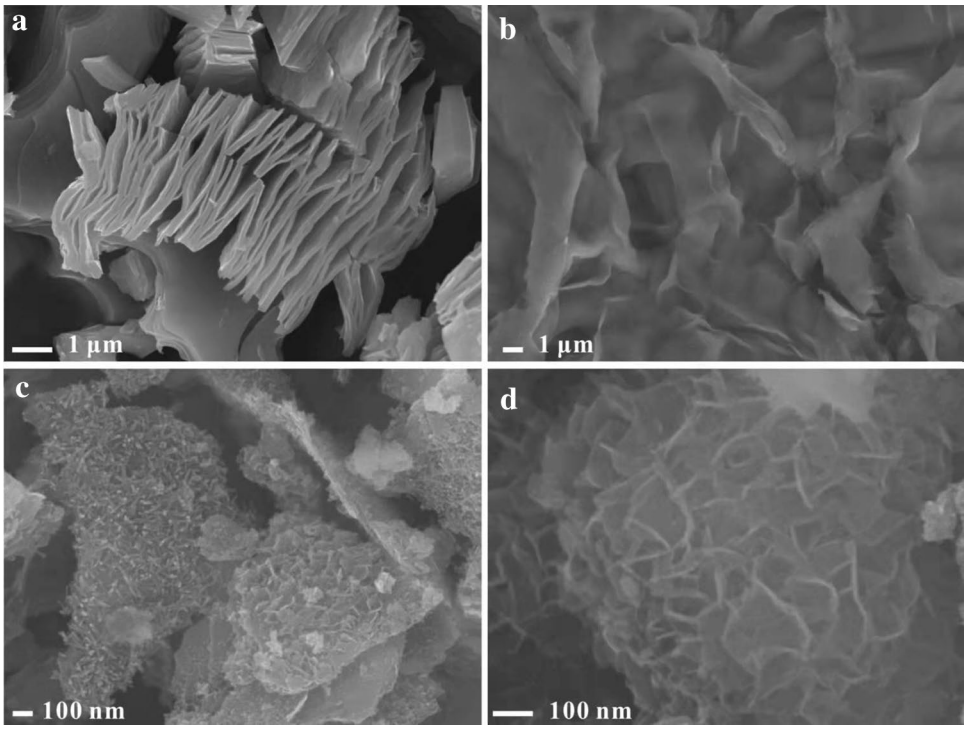

Fig. 2 SEM images of **a** as-synthesized $Ti_3C_2T_x$ MXene, **b** delaminated MXene, **c** and **d** MXene/HS composites

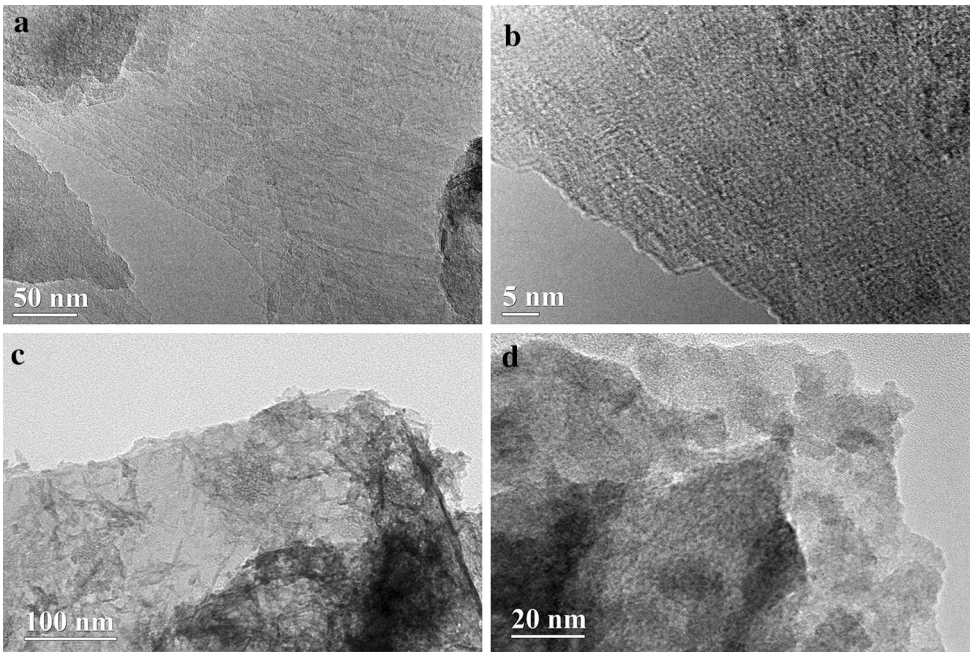

Fig. 3 TEM images of **a**, **b** exfoliated MXene and **c**, **d** MXene/HS composite

XRD pattern of MXene/HS composites displays the typical peaks of HS, demonstrating that HS nanosheets were successfully assembled on the surface of MXene. Moreover, it is noteworthy that the diffraction peak of (002) plane for MXene disappears in the composites, which can be attributed the good separation of MXene nanosheets by anchoring HS nanosheets. In other words, the aggregation of MXene nanosheets was highly prevented by HS nanosheets, which is consistent with SEM and TEM results. Undoubtedly, the introduction of HS plays a vital role in the stabilization of MXene, which will facilitate stable dispersion of the composite in oil.

The surface groups of MXene, HS, and MXene/HS were investigated by FT-IR. As depicted in Fig. 5, the stretching

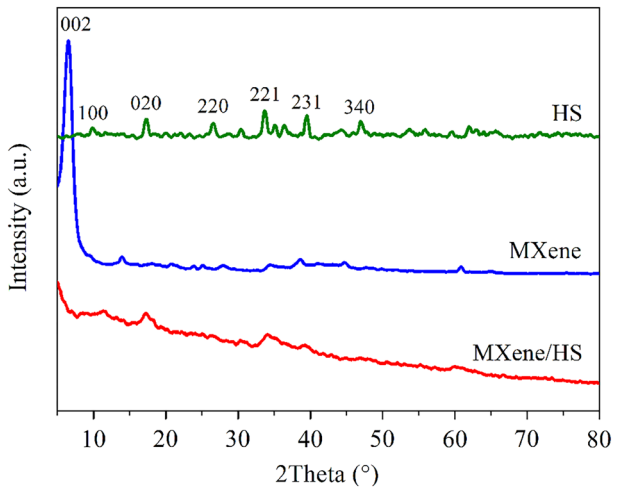

Fig. 4 XRD patterns of MXene, HS, and MXene/HS

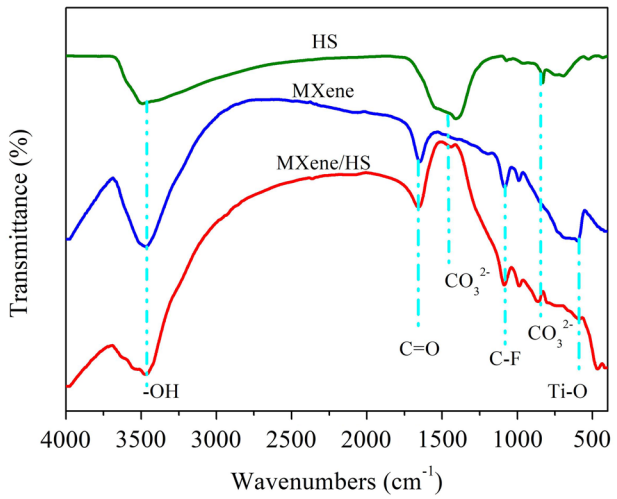

Fig. 5 FT-IR of MXene, HS, and MXene/HS

vibrations of O–H at 3455 cm^{-1} are present in all samples. In addition, the characteristic peaks at 1659 cm^{-1}, 1075 cm^{-1}, and 590 cm^{-1} are ascribed to the stretching of C=O, C–F, and Ti–O, which further confirmed the existence of MXene in the composite [40]. Besides, the peaks centered at 1500 cm^{-1} and 832 cm^{-1} correspond to the stretching vibration of CO_3^{2-}, which appeared in both HS and MXene/HS [34].

The survey XPS spectrum revealed peaks belonging to C, O, Ti, Co and Ni (Fig. 6a). As shown in Fig. 6b, the C 1 s spectrum can be fitted with four peaks at 289.0, 286.27, 284.75, and 281.48 eV, corresponding to O–C=O, C–O, C–C, and C–Ti, respectively [41]. In particular, the O–C=O can be distributed to CO_3^{2-} in the HS. The fitted peaks located at 532.45, 531.8, 531.2, and 529.97 eV can be assigned to metal oxygen bonds (M–O–M), hydroxyl oxygen (–OH), C–Ti–O_x, and Ti–O, respectively [42]. In the Ti 2p spectrum, the deconvoluted peaks mainly correspond to Ti^{2+}, Ti^{3+}, Ti–C, and Ti–O [43]. In addition, there are three peak pairs in the spectrum of Ni 2p (Fig. 6e). Among them, the first doublet centered at 873.46 eV and 855.81 eV and the second centered at 875.16 eV and 857.2 eV are attributed to Ni^{2+} and Ni^{3+} [44], respectively. As for the third pair at 880.45 eV and 861.98 eV, it is related to shakeup satellite peaks. In addition, splitting peaks similar to the Ni 2p orbital can be observed in the spectrum of Co 2p. The Co $2p_{3/2}$ and Co $2p_{1/2}$ orbitals arise at 781.1 eV and 797.0 eV, respectively. Meanwhile, the peaks at 802.75 eV and 786.34 eV correspond to the two shakeup satellites. All relevant data analysis confirmed the successful preparation of MXene/HS composites.

As an additive, homogeneous and stable dispersion in oil needs to be taken into consideration for its practical application. Herein, MXene, HS, and MXene/HS powders were dispersed in PAO-10 base oil by sonication without any organic reagent modification (Fig. 7a). All samples showed a uniform mixture after sonication. However, obvious sedimentation appeared in the suspension of MXene and HS after 10 days. In contrast, the MXene/HS composite was still stably dispersed in the base oil. For the composite, the presence of HS not only helps avoid MXene restacking due to electrostatic repulsion [45], but also the HS nanosheets can act as nanosteric hindrance between MXene nanosheets to alleviate their restacking. Therefore, the composite exhibited better dispersibility than the individual components. The above results implied that compounding is an effective method to create additives with outstanding self-dispersed ability.

The friction and wear behavior of MXene, HS, and MXene/HS as PAO-10 additives were investigated with a ball-on-disk configuration under different normal forces. To determine the optimal concentration of MXene/HS, friction tests with different mass concentrations from 0.1 to 2.0 wt% were operated under 200 N. It is noteworthy that a certain concentration of 1.0 wt% showed better friction-reduction performance (Fig. S4). Subsequently, in view of the limited lubrication performance of PAO-10 oil at high pressure (Fig. S5), the load applied in the experiments was set to 200 N, 250 N, 300 N, and 350 N. Figure 7b–e shows the friction test curves of different samples. In the initial stage, the COF of PAO-10 rose to a high value of 0.6 and then decreased to lower and relatively steady values around 0.16. The high value stage could be attributed to the severe contact pressure of the point contact during the initial running-in conditions. This COF changing tendency of PAO-10 oil is in accordance with the reported results [46, 47]. After adding 1.0 wt% MXene/HS, the lubrication performance was dramatically improved. The COF was steady at approximately 0.12 and running-in period was not observed as the load

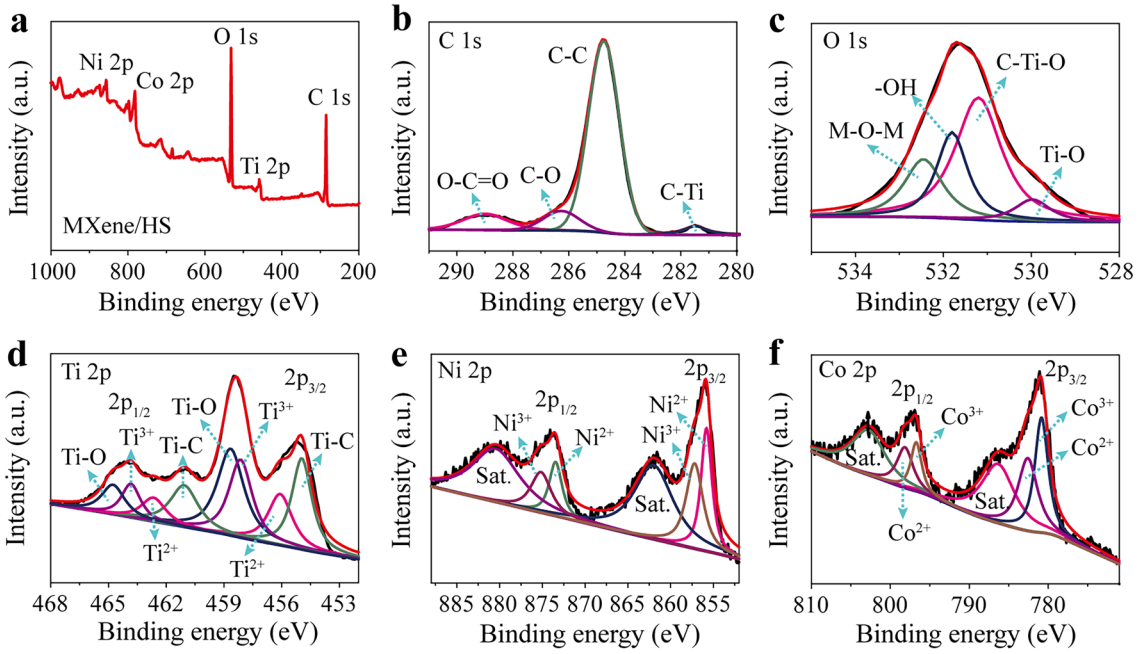

Fig. 6 **a** XPS survey spectrum of MXene/HS composite; high-resolution spectra of **b** C 1 s, **c** O 1 s, **d** Ti 2p, **e** Ni 2p, and **f** Co 2p of MXene/HS composite

changes. Moreover, there was no obvious fluctuation in the friction system lubricated by MXene/HS until the end of sliding. On the other hand, the addition of MXene had a weak effect on the tribological behavior of PAO-10, which was manifested as a slight decrease in COF. Meanwhile, the results also revealed the poor lubrication performance of HS under different loads, which might be caused by the severe agglomeration of HS in the oil (Fig. 7a), causing great difficulty for entering the contact surface of the friction pairs. To intuitively compare the tribological properties of the four samples under different loads, the histograms of average coefficient of friction (ACF) are shown in Fig. 7f. The ACF of the oil sample containing 1 wt% MXene/HS shows a low value and stable tendency, greatly optimizing the friction-reduction property of the base oil. Based on the above analyses, it can be speculated that the self-dispersion ability and anti-aggregation property derived from the formation of composite may be responsible for the improved tribological performance.

To further understand the anti-wear performance of MXene/HS additive, the wear track on the steel disk and wear scar on the steel ball after the friction test are compared in Fig. 8. The width of the worn area lubricated by pure oil was the largest among all samples, with an average width of 949 μm (Fig. 8a1). Moreover, some scratches were beyond the set stroke when lubricated by pure oil, HS, and MXene (Fig. 8a1–a3), indicating the limited tribological properties of these three oil samples and they cannot provide timely feedback in response to sudden sliding [48]. In contrast, the severe wear was not observed for the MXene/HS additive and only narrow (483 μm) wear track was generated, indicating that the substrate was protected by the oil with MXene/HS additive (Fig. 8a4). It can be speculated that MXene/HS could fill the worn defect to decrease the surface roughness and construct a protective film with high strength and great endurance in the friction stage [49, 50]. Wear scars on the steel ball showed the same trend, the scar diameter using pure oil estimated to be approximately 957 μm (Fig. 8b1). However, the oil sample with 1.0 wt% MXene/HS presents the smallest wear scar diameter (Fig. 8b4). The addition of MXene/HS reduces the wear scar diameter by 49.4% compared to that of pure oil (Fig. 8b1–b4). Among these additives, the good compatibility of the composite material with the base oil enables this system to exert the optimum lubricating performance.

3D optical surface measurements were conducted to further evaluate the wear reduction property of the additives. After the friction tests at 300 N, the wear tracks images and corresponding roughness of wear tracks on the steel disk are presented in Fig. 9 and Table S1. After sliding in base oil and oils with MXene and HS additives, many abrasive wear marks were found at contact area of the rubbing steel disk due to the failure of tribofilm (Fig. 9a–c). Compared with the base oil, the worn degree of the contact area with MXene additive was reduced, indicating that MXene can improve the anti-wear performance of the base oil. Evidently, some asperity and deformation appeared at both ends of the tracks, indicating the terrible lubrication conditions in this region

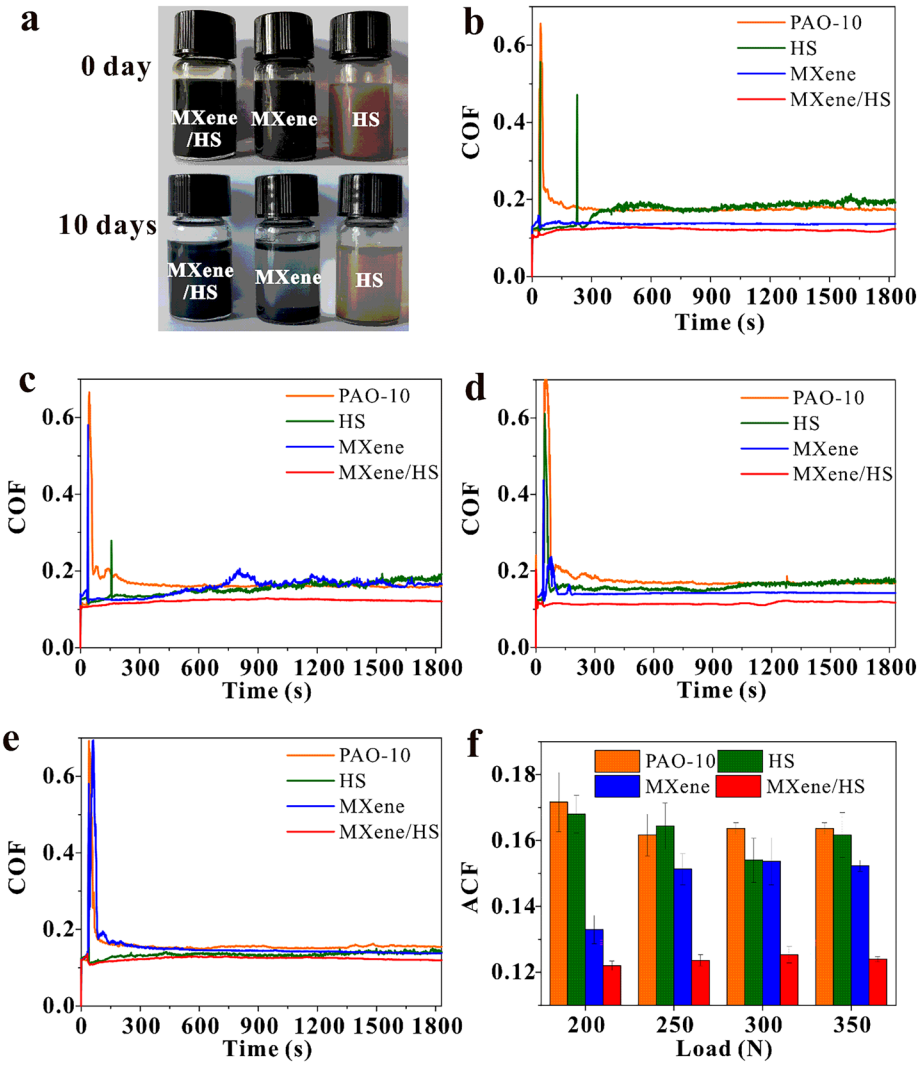

Fig. 7 **a** Photographs of the MXene, HS, and MXene/HS dispersed in PAO-10 base oil at a concentration of 1.0 wt%, taken immediately after sonication and 10 days after sonication, respectively. **b**–**e** Friction curves and **f** ACF using PAO-10 and PAO-10 containing 1.0 wt% MXene, HS, and MXene/HS at different loads of **b** 200 N, **c** 250 N, **d** 300 N, and **e** 350 N, respectively

[51]. The severe deformation phenomenon indicated that a large number of wear particles generated during the sliding process are not conducive to lubrication. As mentioned above, pure base oil and oils with MXene or HS additive cannot effectively resist strong external force extrusion without the aid of proper additives. In contrast, Fig. 9d displays shallow and negligible wear damage in MXene/HS composite lubrication system. When 1.0 wt% MXene/HS was added to oil, the overall wear profile was relatively small and had a regular shape. In addition, there is no serious deformation before and after the wear area, which corresponds to the disappearance of the running-in period in the COF curve. In other words, the lubricating performance of MXene/HS is remarkable, even at the end of the stroke where the lubrication environment is the worst [52]. Besides, the depth of the wear track with MXene/HS additive is approximately 1/5 of the pure base oil (Fig. 9a, d). The calculated wear volume loss after oil formulating with various additives is summarized in Fig. 9e. The corresponding wear volume loss of the steel disk under lubrication of PAO-10 is as high as 2.35×10^6 μm^3 (corresponding to a wear rate of 0.087 μm^3/(N mm), Fig. S6), while the values for that of HS and MXene can be reduced by 16.2% and 23.3%, respectively. When 1.0 wt% MXene/HS composite is added to PAO-10 oil, the wear scar exhibits the smallest wear volume loss of 4.23×10^5 μm^3 (corresponding to a wear rate of 0.016 μm^3/(N mm), Fig. S6; 82.0% reduction). A reasonable explanation for such phenomenon is that the as-synthesized composite additive with self-dispersing ability could more readily penetrate the rubbing contact interface to produce synergistic lubrication with oil during the tribological test.

SEM and EDS analyses of the worn surface were also performed. It can be seen that the rubbed surface lubricated by MXene/HS is relatively smooth as shown in Fig. 10a, b. Meanwhile, some nanoadditives filled in grooves and furrows can be observed as indicated in Fig. 10c, suggesting that MXene/HS composites could play a vital role in lubrication between friction pairs. Furthermore, EDS/EDS mapping

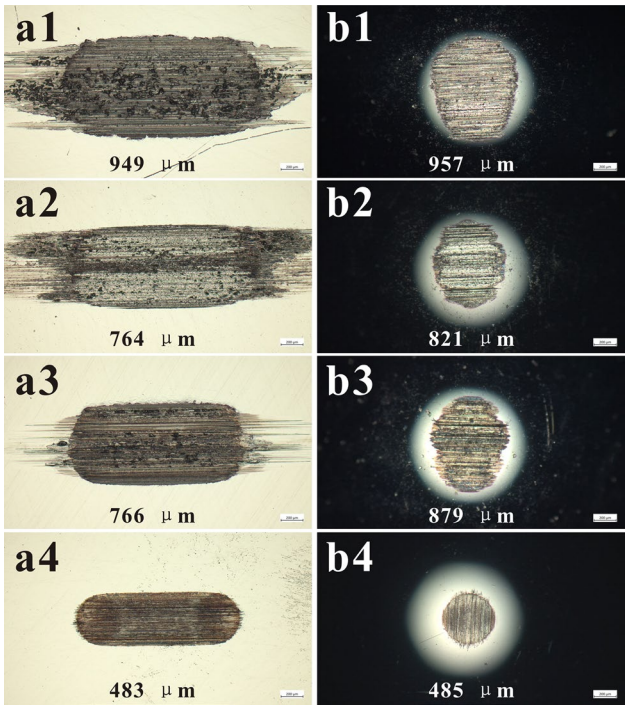

Fig. 8 Optical images of the wear track and wear scar tested with **a1**, **b1** base oil, **a2**, **b2** 1.0 wt% HS, **a3**, **b3** 1.0 wt% MXene, and **a4**, **b4** 1.0 wt% MXene/HS at 300 N

results (Figs. 10d and S7) further confirmed the existence of Ti, F, Ni, and Co elements for the composite additive in this region. These results suggest that MXene/HS composites could be involved in contact interface during the sliding process, leading to the contribution to the antifriction and wear resistance.

To explore the lubrication mechanism, XPS was carried out to determine whether the tribochemical reactions occurred on the worn surface to contribute to the formation of tribofilm. Figure 11 shows the curve-fitted XPS spectra of C 1s, O 1s, Fe 2p, and Ti 2p on the worn steel surfaces lubricated by MXene/HS and MXene. Much stronger XPS signals of C, O, and Ti were detected on the worn surfaces lubricated by MXene/HS than those of lubricated by MXene, indicating that MXene/HS composites were more easily absorbed on the surface of substrate. Under lubrication containing MXene/HS composite additive, the high-resolution XPS spectrum of C 1s (Fig. 11a) can be fitted into three main peaks corresponding to the C–C (284.4 eV), C–O (285.2 eV), and O–C=O (288.4 eV), respectively. The peaks at 529.9, 531.5 and 532.5 eV in the O 1 s spectrum can be assigned to M–O, –OH, and M–O–M, respectively [42]. Besides, two characteristic peaks observed at 529.3 eV and 530.7 eV can be assigned to FeOOH. Similar fitted peaks were observed in the worn surface lubricated by MXene additive, but the peak intensity is significantly

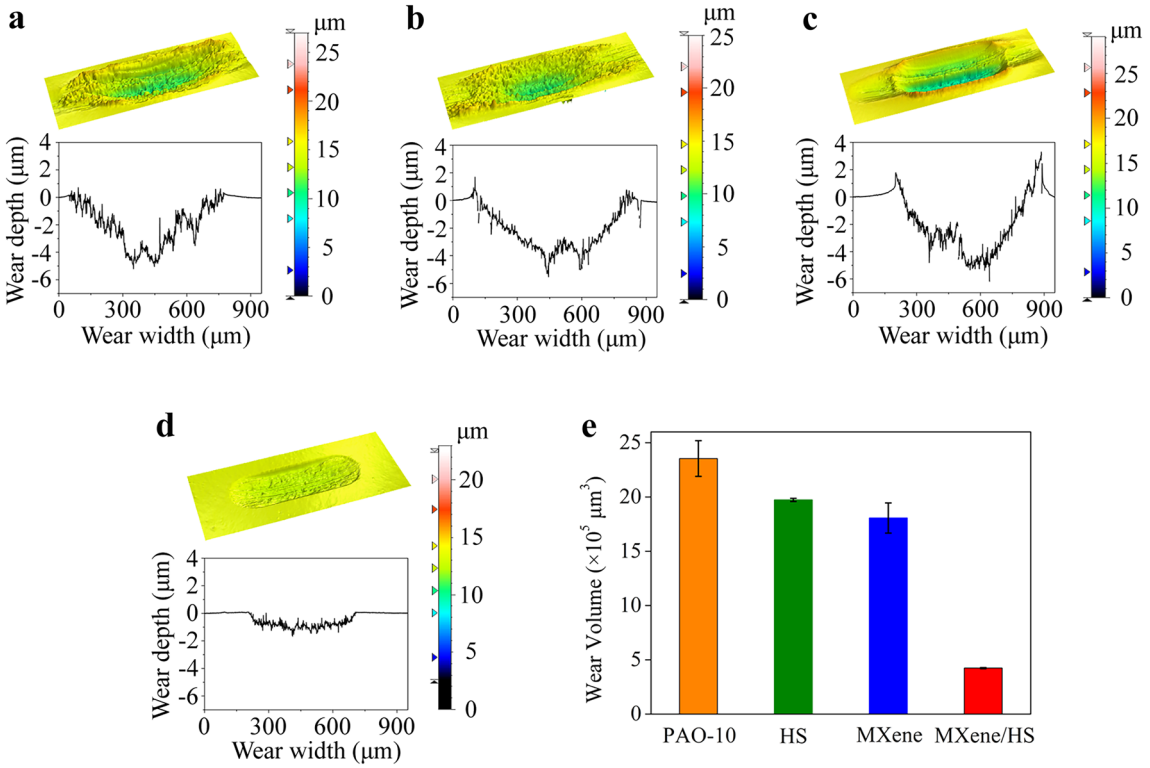

Fig. 9 3D topography and wear depth of the wear tracks lubricated with **a** PAO-10 oil, **b** HS, **c** MXene, and **d** MXene/HS under 300 N. **e** Wear volumes of the different wear tracks

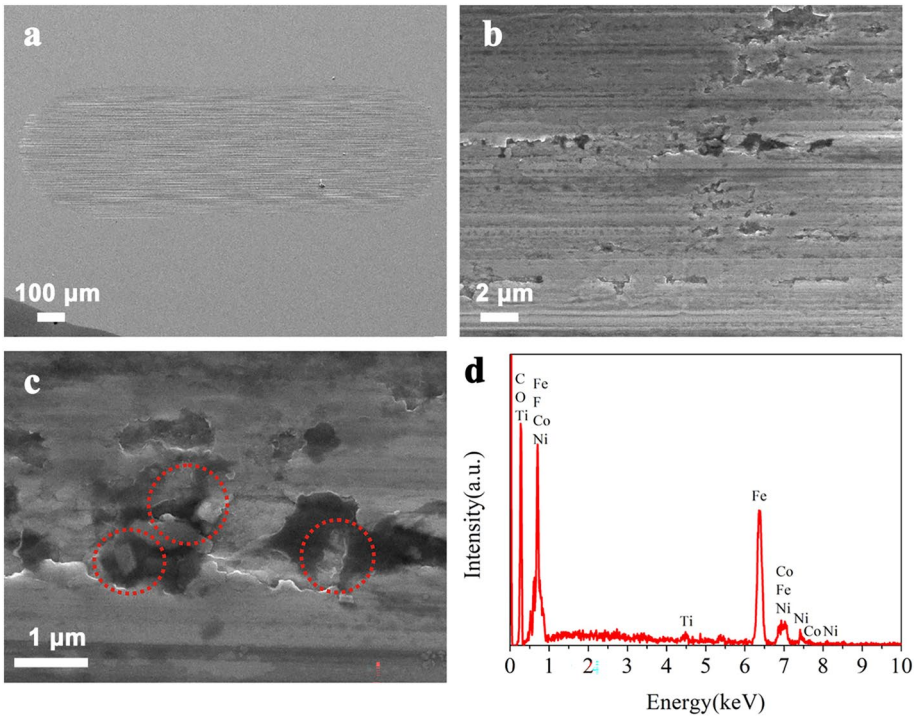

Fig. 10 **a**–**c** SEM images of worn surface lubricated with oil containing MXene/HS composites at different magnification. **d** EDS analysis results of worn surface lubricated with oil containing MXene/HS composites

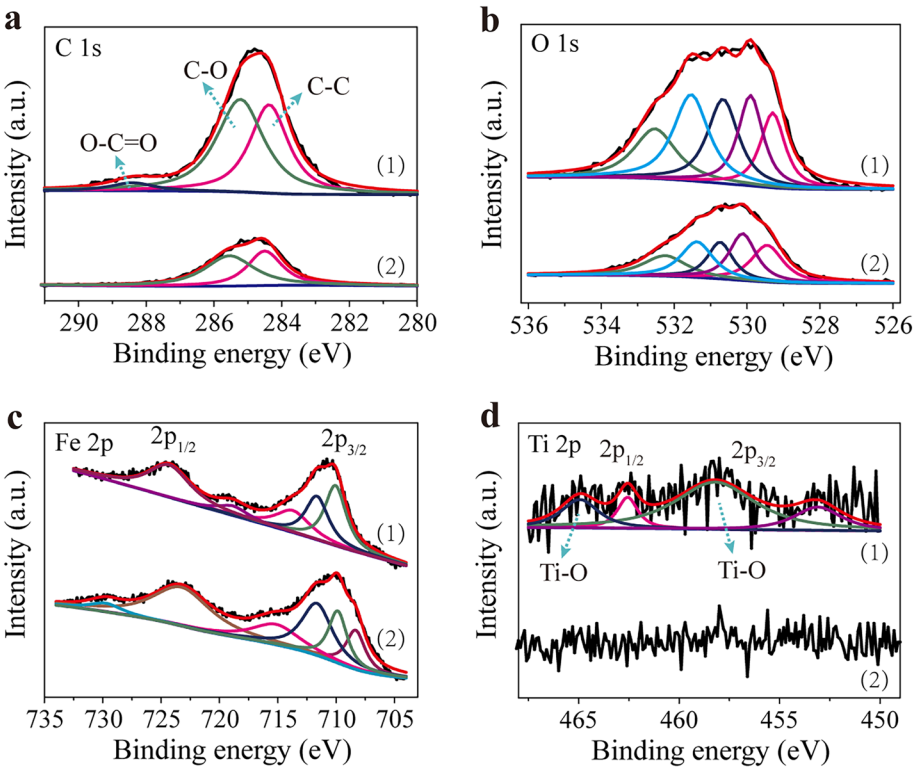

Fig. 11 XPS spectra of **a** C 1s, **b** O 1s, **c** Fe 2p, and **d** Ti 2p of worn track lubricated by (1) MXene/HS composite and (2) MXene

decreased. The stronger signal of O element in the former system indicated that abundant oxidation reactions occurred on the contact surfaces, suggesting that the introduction of HS in composites triggered additional oxidation reactions for promoting the formation of tribofilm. In addition, as presented in Fig. 11c, fitted peaks located at 710.1, 711.6, 713.7, and 724.3 eV are ascribed to a series of oxide species such as FeO, Fe_3O_4, Fe_2O_3, and FeOOH. [51, 53, 54] (detailed assignment is summarized in Table S2), which are similar as the spectrum lubricated by MXene. Notably, for

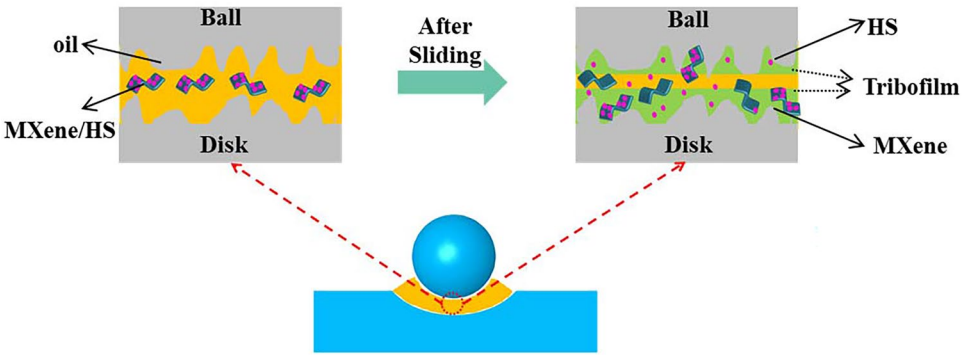

Fig. 12 Lubrication mechanism of sliding contact surface lubricated by MXene/HS composites

the high-resolution XPS spectrum of Ti 2p (Fig. 11d), it only appeared in the spectrum lubricated by MXene/HS. This demonstrates that the MXene/HS additive participated in the rubbing process and a series of oxidation reaction occurred at the worn surfaces. In contrast, MXene additive cannot provide a constant supply of lubrication during sliding due to limited dispersibility. In other words, it is difficult for the stacking MXenes to enter into the contact area to generate sufficient lubrication effect. Based on the above results, it is reasonable to assume that MXene/HS with better dispersion stability could enter the rubbing area to form a surface protective and lubricating film composed of iron and titanium oxides through a series of complex tribochemical reactions. Based on the tribological behavior and XPS data analysis, the composition of the tribofilm formed by MXene/HS is more diverse, and the protection ability for substrate is enhanced compared to the MXene additive.

Based on the surface analyses of wear track, the friction reduction and anti-wear effect can be deduced into following aspects (Fig. 12). First, complete dispersion of MXene/HS composites in PAO-10 base oil can guarantee continuous supply and entry into contact area, which is the primary condition to fully exert their lubrication ability. In contrast, non-functionalized MXenes exhibit short-term stability which also makes them less accessible to the contact area. Second, the interlayer space of MXene nanosheets of the composites was enlarged by the nucleation and growth of HS, leading to the further weakened shear strength and counteracting part of friction force during mechanical movements. Third, the composite additives can embed on the grooves of the rubbing surface spontaneously to decrease roughness. Specifically, HS nanosheets with small size are exfoliated from the composite during the sliding, playing the dual role of sharing the force and filling the grooves. On the other hand, the high temperature generated from friction sliding promotes the adsorption and deposition of additives, forming a dense tribofilm on the worn surface. In this work, the protective tribofilm is not only related to physical adsorption and deposition, but also depends on complex chemical reactions. All in all, the introduction of MXene/HS seems to be a barrier between the friction pairs and prevents the collision of asperities effectively and finally achieving the improvement of the tribological properties.

4 Conclusions

In this paper, self-dispersed MXene/HS composite as additive in PAO-10 was successfully constructed by a facile hydrothermal method. Thanks to the modification with hydroxysalts, the MXene nanosheets are well separated from each other and the resultant composite remains stable in oil. As a lubricant additive, the MXene/HS composite exhibits remarkable antifriction and wear resistance properties. The stable dispersion of the composite ensures the continuous supply during sliding process and facilitates the penetration of lubricating material into the contact area. Moreover, the ideal combination of MXene nanosheets and hydroxysalts creates synergistic lubrication effect via physical interactions and tribochemical reactions. This work enriches the potential application of MXene nanosheets as green additives in tribology and provides inspiration for preparing lubricating materials with outstanding self-dispersing ability.

Supplementary Information The online version contains supplementary material available at https://doi.org/10.1007/s11249-022-01605-3.

Acknowledgements This work was financially supported by the National Natural Science Foundation of China (No. 52175203). Z.L. thanks the Lanzhou Institute of Chemical Physics, CAS for the financial support. T.Z. thanks the financial support from the Natural Science Foundation of Shandong Province, China (No. ZR2019MB062 and ZR2014JL013), and the Key Research and Development Program of Shandong Province (2017GGX20143).

Funding Funding was provided by the National Natural Science Foundation of China (52175203), Natural Science Foundation of Shandong Province (ZR2019MB062 and ZR2014JL013), and Key Research and Development Program of Shandong Province (2017GGX20143).

Declarations

Conflict of interest The authors declare that they have no known competing financial interests or personal relationships that could have appeared to influence the work reported in this paper.

References

1. Holmberg, K., Erdemir, A.: Influence of tribology on global energy consumption, costs and emissions. Friction **5**, 263–284 (2017)
2. Shah, R., Woydt, M., Huq, N., Rosenkranz, A.: Tribology meets sustainability. Ind. Lubr. Tribol. **73**, 430–435 (2021)
3. Gulzar, M., Masjuki, H.H., Kalam, M.A., Varman, M., Zulkifli, N.W.M., Mufti, R.A., Zahid, R.: Tribological performance of nanoparticles as lubricating oil additives. J. Nanopart. Res. **18**, 223 (2016)
4. Liu, L.C., Zhou, M., Jin, L., Li, L.C., Mo, Y.T., Su, G.S., Li, X., Zhu, H.W., Tian, Y.: Recent advances in friction and lubrication of graphene and other 2D materials: mechanisms and applications. Friction **7**, 199–216 (2019)
5. Berman, D., Erdemir, A., Sumant, A.V.: Approaches for achieving superlubricity in two-dimensional materials. ACS Nano **12**, 2122–2137 (2018)
6. Li, W.J., Yang, Z.G., Zha, F., Li, Z., Wang, J.: Preparation of well-dispersed lubricant additives with excellent antiwear ability under high load. Tribol. Lett. **68**, 94 (2020)
7. Liu, Y.F., Ge, X.Y., Li, J.J.: Graphene lubrication. Appl. Mater. Today **20**, 100662 (2020)
8. Zhang, H.: Ultrathin two-dimensional nanomaterials. ACS Nano **9**, 9451–9469 (2015)
9. Wang, W., Xie, G., Luo, J.: Black phosphorus as a new lubricant. Friction **6**, 116–142 (2018)
10. Furlan, K.P., de Mello, J.D.B., Klein, A.N.: Self-lubricating composites containing MoS_2: a review. Tribol. Int. **120**, 280–298 (2018)
11. Zhang, S., Ma, T.B., Erdemir, A., Li, Q.Y.: Tribology of two-dimensional materials: from mechanisms to modulating strategies. Mater. Today **26**, 67–86 (2019)
12. Rosenkranz, A., Liu, Y.Q., Yang, L., Chen, L.: 2D nano-materials beyond graphene: from synthesis to tribological studies. Appl. Nanosci. **10**, 3353–3388 (2020)
13. Zhou, C.Z., Li, Z.P., Liu, S.W., Zhan, T.R., Li, W.Q., Wang, J.Q.: Layered double hydroxides for tribological application: recent advances and future prospective. Appl. Clay Sci. **221**, 106466 (2022)
14. Malaki, M., Varma, R.S.: Mechanotribological aspects of MXene-reinforced nanocomposites. Adv. Mater. **32**, 2003154 (2020)
15. Naguib, M., Mochalin, V.N., Barsoum, M.W., Gogotsi, Y.: 25th anniversary article: MXenes: a new family of two-dimensional materials. Adv. Mater. **26**, 992–1005 (2014)
16. Lin, H., Wang, Y.W., Gao, S.S., Chen, Y., Shi, J.L.: Theranostic 2D tantalum carbide (MXene). Adv. Mater. **30**, 1703284 (2018)
17. Ghidiu, M., Lukatskaya, M.R., Zhao, M.Q., Gogotsi, Y., Barsoum, M.W.: Conductive two-dimensional titanium carbide "clay" with high volumetric capacitance. Nature **516**, 78–81 (2014)
18. Lukatskaya, M.R., Mashtalir, O., Ren, C.E., Dall'Agnese, Y., Rozier, P., Taberna, P.L., Naguib, M., Simon, P., Barsoum, M.W., Gogotsi, Y.: Cation intercalation and high volumetric capacitance of two-dimensional titanium carbide. Science **341**, 1502–1505 (2013)
19. Ran, J.R., Gao, G.P., Li, F.T., Ma, T.Y., Du, A.J., Qiao, S.Z.: Ti_3C_2 MXene co-catalyst on metal sulfide photo-absorbers for enhanced visible-light photocatalytic hydrogen production. Nat. Commun. **8**, 13907 (2017)
20. Wyatt, B.C., Rosenkranz, A., Anasori, B.: 2D MXenes: tunable mechanical and tribological properties. Adv. Mater. **33**, 2007973 (2021)
21. Miao, X.N., Liu, S.W., Ma, L.M., Yang, Y.W., Zhu, J.Y., Li, Z.P., Wang, J.Q.: Ti_3C_2-graphene oxide nanocomposite films for lubrication and wear resistance. Tribol. Int. **167**, 107361 (2022)
22. Grutzmacher, P.G., Suarez, S., Tolosa, A., Gachot, C., Song, G.C., Wang, B., Presser, V., Muecklich, F., Anasori, B., Rosenkranz, A.: Superior wear-resistance of Ti_3C_2Tx multilayer coatings. ACS Nano **15**, 8216–8224 (2021)
23. Marian, M., Feile, K., Rothammer, B., Bartz, M., Wartzack, S., Seynstahl, A., Tremmel, S., Krauss, S., Merle, B., Bohm, T., Wang, B., Wyatt, B.C., Anasori, B., Rosenkranz, A.: Ti_3C_2Tx solid lubricant coatings in rolling bearings with remarkable performance beyond state-of-the-art materials. Appl. Mater. Today **25**, 101202 (2021)
24. Yin, X., Jin, J., Chen, X.C., Rosenkranz, A., Luo, J.B.: Ultra-wear-resistant MXene-based composite coating via in situ formed nanostructured tribofilm. ACS Appl. Mater. Interfaces **11**, 32569–32576 (2019)
25. Huang, S., Mutyala, K.C., Sumant, A.V., Mochalin, V.N.: Achieving superlubricity with 2D transition metal carbides (MXenes) and MXene/graphene coatings. Mater. Today Adv. **9**, 100133 (2021)
26. Gao, J.D., Du, C.F., Zhang, T.T., Zhang, X.Z., Ye, Q., Liu, S.J., Liu, W.M.: Dialkyl dithiophosphate-functionalized Ti_3C_2Tx MXene nanosheets as effective lubricant additives for antiwear and friction reduction. ACS Appl. Nano Mater. **4**, 11080–11087 (2021)
27. Feng, Q., Deng, F.K., Li, K.C., Dou, M.Y., Zou, S., Huang, F.C.A.: Enhancing the tribological performance of Ti_3C_2 MXene modified with tetradecylphosphonic acid. Colloids Surf. A. **625**, 126903 (2021)
28. Zhao, J., Huang, Y.Y., He, Y.Y., Shi, Y.J.: Nanolubricant additives: a review. Friction **9**, 891–917 (2021)
29. Liu, Y., Zhang, X.F., Dong, S.L., Ye, Z.Y., Wei, Y.D.: Synthesis and tribological property of Ti_3C_2Tx nanosheets. J. Mater. Sci. **52**, 2200–2209 (2017)
30. Zhang, X.F., Guo, Y., Li, Y.J., Liu, Y., Dong, S.L.: Preparation and tribological properties of potassium titanate-Ti_3C_2Tx nanocomposites as additives in base oil. Chin. Chem. Lett. **30**, 502–504 (2019)
31. Dou, X., Koltonow, A.R., He, X.L., Jang, H.D., Wang, Q., Chung, Y.W., Huang, J.X.: Self-dispersed crumpled graphene balls in oil for friction and wear reduction. Proc. Natl. Acad. Sci. USA **113**, 1528–1533 (2016)
32. Wang, L., Gong, P.W., Li, W., Luo, T., Cao, B.Q.: Mono-dispersed Ag/Graphene nanocomposite as lubricant additive to reduce friction and wear. Tribol. Int. **146**, 106228 (2020)
33. Ramesh, T.N.: Observation of polytypism among the hydroxysalts of Ni(II) and Co(II). Inorg. Chem. Commun. **12**, 832–834 (2009)
34. Xing, W., Zhuo, S., Cui, H., Zhou, H., Si, W., Yuan, X., Gao, X., Yan, Z.: Morphological control in synthesis of cobalt basic carbonate nanorods assembly. Mater. Lett. **62**, 1396–1399 (2008)
35. Ballesteros, M.A., Ulibarri, M.A., Rives, V., Barriga, C.: Optimum conditions for intercalation of lacunary tungstophosphate(V) anions into layered Ni(II)-Zn(II) hydroxyacetate. J. Solid State Chem. **181**, 3086–3094 (2008)
36. Kamath, P.V., Dixit, M., Indira, L., Shukla, A.K., Kumar, V.G., Munichandraiah, N.: Stabilized α-$Ni(OH)_2$ as electrode material for alkaline secondary cells. J. Electrochem. Soc. **141**, 2956–2959 (1994)
37. Kumar, J.A., Prakash, P., Krithiga, T., Amarnath, D.J., Premkumar, J., Rajamohan, N., Vasseghian, Y., Saravanan, P., Rajasimman, M.: Methods of synthesis, characteristics, and environmental

applications of MXene: a comprehensive review. Chemosphere **286**, 131607 (2022)
38. Alhabeb, M., Maleski, K., Anasori, B., Lelyukh, P., Clark, L., Sin, S., Gogotsi, Y.: Guidelines for synthesis and processing of two-dimensional titanium carbide (Ti_3C_2Tx MXene). Chem. Mater. **29**, 7633–7644 (2017)
39. Zheng, J.L., Pan, X., Huang, X.M., Xiong, D.B., Shang, Y., Li, X.X., Wang, N., Lau, W.M., Yang, H.Y.: Integrated $NiCo_2$-LDHs@MXene/rGO aerogel: componential and structural engineering towards enhanced performance stability of hybrid supercapacitor. Chem. Eng. J. **396**, 125197 (2020)
40. Chen, J.F., Zhao, W.J.: Simple method for preparing nanometer thick Ti_3C_2Tx sheets towards highly efficient lubrication and wear resistance. Tribol. Int. **153**, 106598 (2021)
41. Gao, X.R., Jia, Z.R., Wang, B.B., Wu, X.M., Sun, T., Liu, X.H., Chi, Q.G., Wu, G.L.: Synthesis of NiCo-LDH/MXene hybrids with abundant heterojunction surfaces as a lightweight electromagnetic wave absorber. Chem. Eng. J. **419**, 130019 (2021)
42. Qu, Y.P., Shi, C.J., Cao, H.F., Wang, Y.Z.: Synthesis of Ni-MOF/Ti_3C_2Tx hybrid nanosheets via ultrasonific method for supercapacitor electrodes. Mater. Lett. **280**, 128526 (2020)
43. Wang, W.D., Jiang, D.M., Chen, X., Xie, K., Jiang, Y.H., Wang, Y.Q.: A sandwich-like nano-micro LDH-MXene-LDH for high-performance supercapacitors. Appl. Surf. Sci. **515**, 145982 (2020)
44. Huang, X.Y., Chi, Z.T., Liu, J., Li, D.H., Sun, X.J., Yan, C., Wang, Y.C., Li, H., Wang, X.D., Xie, W.F.: Enhanced gas sensing performance based on p-NiS/n-In_2O_3 heterojunction nanocomposites. Sens. Actuators B **304**, 127305 (2020)
45. Quero, F., Rosenkranz, A.: Mechanical performance of binary and ternary hybrid MXene/nanocellulose hydro- and aerogels—a critical review. Adv. Mater. Interfaces **8**, 2100952 (2021)
46. Wen, P., Zhang, C.Y., Yang, Z.G., Dong, R., Wang, D.M., Fan, M.J., Wang, J.Q.: Triazine-based covalent-organic frameworks: a novel lubricant additive with excellent tribological performances. Tribol. Int. **111**, 57–65 (2017)
47. Wu, X.H., Gong, K.L., Zhao, G.Q., Lou, W.J., Wang, X.B., Liu, W.M.: Surface modification of MoS_2 nanosheets as effective lubricant additives for reducing friction and wear in poly-alpha-olefin. Ind. Eng. Chem. Res. **57**, 8105–8114 (2018)
48. Huang, H.D., Tu, J.P., Gan, L.P., Li, C.Z.: An investigation on tribological properties of graphite nanosheets as oil additive. Wear **261**, 140–144 (2006)
49. Chang, Q.Y., Rudenko, P., Miller, D.J., Wen, J.G., Berman, D., Zhang, Y.P., Arey, B., Zhu, Z.H., Erdemir, A.: Operando formation of an ultra-low friction boundary film from synthetic magnesium silicon hydroxide additive. Tribol. Int. **110**, 35–40 (2017)
50. Yu, Q.L., Li, D.M., Cai, M.R., Zhou, F., Liu, W.M.: Supramolecular gel lubricants based on amino acid derivative gelators. Tribol. Lett. **61**, 16 (2016)
51. Ye, Q., Liu, S., Zhang, J., Xu, F., Zhou, F., Liu, W.M.: Superior lubricity and antiwear performances enabled by porous carbon nanospheres with different shell microstructures. ACS Sustain. Chem. Eng. **7**, 12527–12535 (2019)
52. Qu, J., Truhan, J.J., Blau, P.J., Meyer, H.M.: Scuffing transition diagrams for heavy duty diesel fuel injector materials in ultra low-sulfur fuel-lubricated environment. Wear **259**, 1031–1040 (2005)
53. Hou, K.M., Wang, J.Q., Yang, Z.G., Ma, L.M., Wang, Z.F., Yang, S.R.: One-pot synthesis of reduced graphene oxide/molybdenum disulfide heterostructures with intrinsic incommensurateness for enhanced lubricating properties. Carbon **115**, 83–94 (2017)
54. Ye, Q., Liu, S., Xu, F., Zhang, J., Liu, S.J., Liu, W.M.: Nitrogen-phosphorus codoped carbon nanospheres as lubricant additives for antiwear and friction reduction. ACS Appl. Nano. Mater. **3**, 5362–5371 (2020)

Authors and Affiliations

Changzhi Zhou[2] · Zhangpeng Li[1,3,4] · Shuwen Liu[1,4] · Limin Ma[1] · Tianrong Zhan[2] · Jinqing Wang[1]

[1] State Key Laboratory of Solid Lubrication, Lanzhou Institute of Chemical Physics, Chinese Academy of Sciences, Lanzhou 730000, China

[2] Key Laboratory of Optic-Electric Sensing and Analytical Chemistry for Life Science (Ministry of Education), State Key Laboratory Base of Eco-Chemical Engineering, Qingdao University of Science and Technology, Qingdao 266042, China

[3] Yantai Zhongke Research Institute of Advanced Materials and Green Chemical Engineering, Yantai 264006, China

[4] Qingdao Center of Resource Chemistry & New Materials, Qingdao 266000, China